

# Firing-rate resonances in the peripheral auditory system of the cricket, *Gryllus bimaculatus*

Florian Rau<sup>1</sup> · Jan Clemens<sup>1,2</sup> · Victor Naumov<sup>1</sup> · R. Matthias Hennig<sup>1</sup> · Susanne Schreiber<sup>2,3</sup>

Received: 27 April 2015 / Revised: 3 August 2015 / Accepted: 4 August 2015 / Published online: 21 August 2015  
© Springer-Verlag Berlin Heidelberg 2015

**Abstract** In many communication systems, information is encoded in the temporal pattern of signals. For rhythmic signals that carry information in specific frequency bands, a neuronal system may profit from tuning its inherent filtering properties towards a peak sensitivity in the respective frequency range. The cricket *Gryllus bimaculatus* evaluates acoustic communication signals of both conspecifics and predators. The song signals of conspecifics exhibit a characteristic pulse pattern that contains only a narrow range of modulation frequencies. We examined individual neurons (AN1, AN2, ON1) in the peripheral auditory system of the cricket for tuning towards specific modulation frequencies by assessing their firing-rate resonance. Acoustic stimuli with a swept-frequency envelope allowed an efficient characterization of the cells' modulation transfer functions. Some of the examined cells exhibited tuned band-pass properties. Using simple computational models, we demonstrate how different, cell-intrinsic or network-based mechanisms such as subthreshold resonances, spike-triggered adaptation, as well as an interplay of excitation and inhibition can account for the experimentally observed firing-rate resonances. Therefore, basic neuronal mechanisms that share negative feedback as a common theme may contribute to selectivity in the peripheral auditory pathway

of crickets that is designed towards mate recognition and predator avoidance.

**Keywords** Auditory processing · Acoustic communication · Neuron models · Band-pass filtering · Negative feedback

## Introduction

Tuned filters play a vital role in communication: in order to accurately receive a signal through a noisy channel, the receiving side benefits from narrowing and centering perception to the spectral characteristics of the signal. This also applies to neuronal communication (Borst and Theunissen 1999). Obvious examples are linked to sensory systems, where highly convergent signal pathways reduce the broad information from the outside world to a manageable stream of information (Barlow 1961). Here, resonances equip neurons with the ability to resolve and efficiently encode spectral components of a stimulus—take, for instance, the Gabor filters proposed for the mammalian visual (Hubel and Wiesel 1962; Jones and Palmer 1987) and auditory system (Smith and Lewicki 2006), or the electrical tuning of hair cells in lower vertebrates (Fettiplace 1987).

Neuronal filtering plays a decisive role in specialized sensory systems. For sensory systems that are dedicated to detecting a narrow range of stereotyped signals, one can—on an evolutionary timescale—expect filtering to be optimized for an efficient and reliable processing of signals (Cariani 2001). The spectral tuning of neurons poses an obvious target for selection. In particular, when the size of neuronal circuits is constrained (like in the case of insects) and the behaviorally most relevant signals are rhythmic, the

✉ Florian Rau  
florian.rau@hu-berlin.de

<sup>1</sup> Behavioral Physiology, Department of Biology, Humboldt-Universität zu Berlin, Invalidenstr. 43, 10115 Berlin, Germany

<sup>2</sup> Bernstein Center for Computational Neuroscience Berlin, Unter den Linden 6, 10099 Berlin, Germany

<sup>3</sup> Institute for Theoretical Biology, Department of Biology, Humboldt-Universität zu Berlin, Philippstr. 13, Haus 4, 10115 Berlin, Germany

implementation of bandpass-like filter properties may pose an attractive coding strategy.

Here, we investigate tuning properties of neurons in the size-constrained peripheral auditory network of crickets, aiming to understand whether the frequency dependence of signal processing in this small entrance circuit is already tailored to the rhythmic structure of vital communication signals. To this end, we focus on “firing-rate resonances”, that is, bandpass-like frequency dependences of neuronal firing-rate transfer functions. Specifically, such resonances are reflected in largest firing-rate responses to inputs in a selected frequency band. Beyond the specific physiology and network architecture of the cricket’s peripheral auditory pathway, we examine three conceptually different mathematical model types that can describe the observed firing-rate resonances. We seek to understand to what extent these different mechanisms can capture general, quantitative aspects of the recorded firing-rate resonances.

Female crickets recognize and selectively track the rhythmic calling songs of conspecific males (Bennet-Clark 1989) in a behavior known as phonotaxis (Popov et al. 1976). Due to the behavioral importance of these songs and their rhythmicity, an early specialization of peripheral neurons onto relevant frequency ranges may be an efficient computational strategy (Tunstall and Pollack 2005). In the cricket’s brain, several higher-order neurons exhibit their highest firing rates in response to acoustic stimuli that match the temporal features of the cricket’s song (Schildberger 1984; Kostarakos and Hedwig 2012). The sharpness of this modulation tuning appears to increase from neuron to neuron in sequence of processing (Schildberger 1984; Kostarakos and Hedwig 2012), hinting towards a distributed, cumulative filtering. The underlying filtering mechanisms, however, are still debated: concepts include template matching (Hoy 1978; Hennig 2003), delay lines (Reiss 1962; Weber and Thorson 1989; Kostarakos and Hedwig 2015), neural resonance (Eilts-Grimm and Wiese 1984; Bush and Schul 2006; Webb et al. 2007) and band-pass formation through interaction of low- and high-pass neurons (Schildberger 1984).

We utilized a novel, efficient stimulation paradigm to demonstrate that—even in the auditory periphery—some of the examined neurons acted as tuned filters, yielding highest firing-rates in response to the modulation frequencies characteristic of the male crickets’ mating song. Across cell types, we find that firing-rate resonances are expressed with different strengths and frequency preferences, consistent with previous studies involving other species and measures (Nabatiyan et al. 2003; Marsat and Pollack 2004; Tunstall and Pollack 2005). Guided by the experimentally recorded firing-rate resonance in one of the cricket neuron types, we proceed to a more general level to compare how different, previously described mechanisms in single cells or small

circuits can quantitatively account for the observed firing-rate resonances. The computational approach comprises (1) a model with subthreshold resonance of the membrane impedance in a single cell, (2) a model with spike-triggered adaptation in a single cell, as well as (3) small network models with delayed inhibition or specialized cut-off frequencies. Despite differences in the underlying components, all mechanisms share the principle of negative feedback and we find that they capture the firing-rate resonance well. We conclude that these biophysical and network mechanisms are interesting candidates for firing-rate resonances in invertebrate systems and may be useful for the description of firing-rate resonances beyond the specifics of the cricket system analyzed in this study.

## Material and methods

### Experiment

#### Preparation

Laboratory-reared female crickets of the species *Gryllus bimaculatus* were used in all experiments. After visually inspecting the intactness of the tympana, both meso- and metathoracic legs as well as the wings were removed and the animal was fixed ventral side up to a recording stage using bees wax. The front legs were fixed in a walking position while care was taken not to constrict the tympana with wax. In order to reduce overall neuronal activity and body movements, both the meso- and the metathoracic ganglion were removed and the connectives between prothoracic and suboesophageal ganglion were cut. Maxillae, labium and gut were removed. All cuts were sealed with a viscous mixture of petroleum jelly and mineral oil to provide electrical insulation and prevent the preparation from drying out.

#### Electrophysiology

Signals from AN1 and AN2 were recorded differentially (EXT-10C, npi electronics, Tamm, Germany) from one of the connectives between prothoracic and suboesophageal ganglion using tungsten hook electrodes, referenced to a silver wire in the animal’s abdomen (Hennig 1988). Signals from ON1 were recorded in separate sessions from the prothoracic ganglion using a 500 k $\Omega$  extracellular tungsten electrode (World Precision Instruments, Sarasota, FL, USA) referenced to a stabilizing metal spatula. ON1 was identified by its greater sensitivity, but longer response latency, to stimulation at 4.5 kHz compared to 16 kHz (for *Teleogryllus oceanicus*: Faulkes and Pollack 2000; Sabourin et al. 2008). Voltage signals were band-pass filtered

between 300 and 3000 Hz (DPA-2FX, npi electronics), digitized at 20 kS/s (PCI-6229, National Instruments, Austin, TX, USA) and recorded to the hard disk of a desktop computer using custom software (LabView, National Instruments).

*Stimulation*

To efficiently sample both spike rate and spike timing responses across a range of frequencies, we employed acoustic stimuli with a swept-frequency amplitude modulation (SFAM). The envelope function of SFAM stimuli resembled a sinusoidal wave whose instantaneous frequency  $f_{AM}(t)$  changed linearly with time:

$$f_{AM}(t) = f_0 + \beta t, \quad \beta = \frac{f_1 - f_0}{t_1}, \quad (1)$$

where  $f_0$  was the initial frequency at time  $t = 0$ s,  $f_1$  was the target frequency at stimulus duration  $t_1$  and  $\beta$  was the sweep rate; that is, the slope of  $f_{AM}(t)$ . The amplitude of the envelope function followed:

$$y(t) = \frac{1}{2} \cos \left[ 2\pi \left( f_0 t + \frac{\beta}{2} t^2 \right) + \pi \right] + \frac{1}{2}.$$

We used stimuli with the parameters  $t_1 = 10$  s,  $f_0 = 1$  Hz and  $f_1 = 100$  Hz, which resulted in a sweep rate of  $\beta = 9.9$  Hz/s. For AN1 and AN2 we also used additional stimuli with a shorter duration ( $t_1 = 5$  s) and frequencies ranging from  $f_0 = 0$  Hz to either  $f_1 = 50$  Hz or  $f_1 = 500$  Hz (yielding chirp rates of  $\beta = 10$  Hz/s and  $\beta = 100$  Hz/s, respectively). To account for effects of adaptation, stimuli were also presented in reverse, that is, with falling instantaneous frequencies.

Throughout the cricket’s auditory system one can observe a dichotomy between pathways that are sensitive to low carrier frequencies and those that are sensitive to high carrier frequencies (Popov et al. 1976; Boyan and Williams 1982; Schildberger 1984). In order to adequately stimulate both pathways, envelope functions were multiplied with sine carriers of either 4.5 or 16 kHz, coinciding with the respective characteristic frequencies of the ascending neurons AN1 and AN2 (Fig. 1 in Rheinlaender et al. 1976; Fig. 2 in Schildberger 1984). Stimuli were computed at a resolution of 100 kHz. After digital-to-analog conversion (PCI-6229, National Instruments), stimuli were adjusted to a peak intensity of 80 dB SPL (ATN-01M, npi electronics), amplified with a power amplifier (Raveland XA-600, Blaupunkt, Hildesheim, Germany) and presented via one of two loudspeakers mounted at a distance of 30 cm and an angle of 90° to either side of the animal’s longitudinal body axis. Stimuli were presented in randomized order with each stimulus being presented up to 25 times, depending on the state of the recording.

**Data processing**

*Spike detection*

Spike times were extracted from the raw voltage traces by means of a basic threshold detection method (Benda and Hennig 2008). Distributions of inter spike intervals (ISIs) were used to assess the quality of extracted spike times. In three recordings within the prothoracic ganglion, low ISIs indicated multi-unit activity originating from the mirror-image pair of ON1-type neurons (cf. Wohlers and Huber 1982). In these cases we used a more advanced method of spike sorting based on wavelet decomposition and superparamagnetic clustering adapted from Quiroga et al. (2004), allowing for a good separation of the two cells’ spike shapes. All spike times were corrected for median first-spike latencies to 80 dB SPL pulses of the respective carrier frequencies. We obtained a total of 8 datasets from AN1, 11 from AN2 and 10 from ON1.

*Modulation transfer functions*

The SFAM stimulation protocol delivered a linear sweep of modulation frequencies, with each stimulus segment representing a defined frequency band. We exploited this property by analyzing the experimentally obtained data with a sliding window approach. The procedure yielded two common measures for characterizing the relationship between the stimulus’ amplitude modulations and the recorded firing events, namely (1) the *rate* modulation transfer function (rMTF), and (2) the *temporal* modulation transfer function (tMTF). The two measures describe the AM frequency transfer on the levels of average and stimulus locked firing respectively (Eggermont and Wang 2011).

In order to obtain the two kinds of MTFs, we first converted the recorded spike times into binary spike trains (waveforms at the 20 kHz sampling rate of the original recordings with *zero* representing “no spike” and *one* representing “spike”). These row vectors were averaged across trials and multiplied by their sampling rate, essentially yielding the numerical representation of a highly resolved peristimulus time histogram (PSTH, Gerstein and Kiang 1960) with a bin size equal to the reciprocal of the recording’s sampling rate.

From these data, MTFs were obtained by means of the short-time Fourier transform (STFT)—a Fourier-related transform that captures the spectral properties of a local section of a signal. The discrete STFT corresponds to a regular discrete Fourier transform (DFT) but combines the sampled signal  $x(m)$  with a window function  $w(m)$ :

$$X(n, k) = \sum_{m=0}^{N-1} x(m)w(n - m) \cdot e^{-i\frac{2\pi}{N}km}, \quad k \in \mathbb{Z},$$

where  $f(m) = x(m)w(n - m)$  is a short-time section of signal  $x(m)$  at time  $n$ ,  $N$  is the length of  $x(m)$  and  $k$  is the index of the DFT coefficient to be calculated.

The *rate* modulation transfer function (rMTF) describes a cell's mean firing rate as a function of AM frequency (Schreiner and Langner 1988). In the frequency domain, the mean value of a signal is given by the spectral magnitude at 0 Hz, the DC bias. The corresponding STFT at  $k = 0$  reduces to a convolution of signal  $x$  and window  $w$ :

$$\begin{aligned} \text{rMTF}(t) &= |X(tf_s, 0)|, \\ &= \sum_{m=0}^{N-1} x(m)w(tf_s - m), \end{aligned}$$

where  $f_s$  is the sampling rate of the recording. Thus, in this case the STFT was merely used for smoothing the highly resolved PSTH from the previous step.

The *temporal* modulation transfer function (tMTF) characterizes a cell's ability to synchronize its firing to the amplitude modulations of a stimulus (Schreiner and Langner 1988). It can be expressed both in absolute or relative terms (Eggermont and Wang 2011). The relative measure is commonly known as the vector strength (VS). Here, however, the tMTF is defined as an absolute measure of phase-locked firing rate; that is, the magnitude of the response's Fourier component at the stimulus' instantaneous AM frequency:

$$\text{tMTF}(t) = |X[tf_s, k_{\text{AM}}(t)]|,$$

where  $k_{\text{AM}}(t)$  is the DFT index that corresponds to the stimulus envelope's instantaneous frequency  $f_{\text{AM}}(t)$  (see Eq. 1):

$$k_{\text{AM}}(t) = \left\lfloor N \cdot \frac{f_{\text{AM}}(t)}{f_s} \right\rfloor.$$

For both MTFs, a flat top window (Gade and Herlufsen 1987) was used, with width  $\sigma = 1$  s (for  $\beta \leq 10$  Hz/s) or  $\sigma = 300$  ms (for  $\beta = 100$  Hz/s) and 90 % overlap. Overall, the positions of transfer peaks were relatively independent of the window's width in a range of  $\pm 50\%$ . More narrow windows, however, were avoided, as they undersampled the neurons' low-frequency response and led to aliasing. For an efficient and accurate evaluation of the individual DFT terms we employed the Goertzel algorithm (Goertzel 1958; section 3.4 in Sysel and Rajmic 2012).

The two measures correspond to cross-sections of the spike train's magnitude spectrogram along the DC component and along the stimulus envelope's fundamental frequency, as illustrated in Fig. 2. While the rMTF quantifies mean firing rates much like a regular PSTH, the tMTF represents the absolute rate contribution of spikes that are phase-locked to the stimulus' instantaneous modulation frequency.

### Detection and characterization of transfer peaks

The position and shape of transfer peaks were characterized across recordings. To this end, both the respective rMTF and tMTF were fitted with cubic smoothing splines (smoothing parameter  $p = 0.02$ , average  $R^2 = 0.99$ ), extrapolated to 0 Hz and processed with a peak detection algorithm (Todd and Andrews 1999). Peaks in the smoothed transfer functions were included in further analyses, if they rose above adjacent troughs by an amplitude factor of 1.1 or higher. They were characterized by the peak frequency  $f_p$  and the quality factor  $Q$ , the latter defined as the ratio between the magnitude at  $f_p$  and the extrapolated magnitude at 0 Hz (Koch 1984; Hutcherson et al. 1996). For transfer functions that merely exhibit a lowpass dependence on modulation frequency, the peak frequency  $f_p$  coincides with 0 Hz and, thus,  $Q$  equals 1. Transfer functions are characterized by a  $Q$  value greater 1, if they exhibit a peaked (i.e., resonant) dependence on modulation frequency. Note, that the  $Q$  value applied here differs from a homonymous measure for characterizing resonant systems, defined as the ratio of peak frequency and bandwidth (cf. Hennig et al. 2004).

### Models

We implemented three conceptually different models that reproduce the observed firing-rate resonances in the prothoracic network of the cricket. The models were not meant to accurately represent the cricket's auditory physiology but rather served to illustrate how general cellular mechanisms could lead to firing-rate resonances. For this reason, the number of model parameters was deliberately kept low. Moreover, the models are of phenomenological nature. The parameters hence cannot be expected to agree with detailed biophysical or electrophysiological parameters of the crickets' neurons in a one-to-one manner. While we tried to place the model parameters in a realistic order of magnitude (cf. van Hateren and Laughlin 1990; Borst and Haag 1996), they do not represent a measurement-based, quantitative estimate of the corresponding parameters in the cricket's nervous system.

As input to all models we used scaled envelope functions, as the cricket's auditory receptors code for amplitude modulation (Machens et al. 2001; Imaizumi and Pollack 2001). To best illustrate the models' own filtering capabilities, we disregarded both the individual and combined transfer characteristics of the cricket's populations of auditory receptors (Sabourin and Pollack 2010; Sharafi et al. 2013) and assumed unfiltered inputs. Models were manually tuned to match both peak frequency and  $Q$  value of ON1's average rMTF ( $f_p = 23.9$  Hz,  $Q = 1.34$ ; cf. Fig. 3d) within a tolerance of 1.5 %. All modeling was performed with custom-written routines in MATLAB (MathWorks, Natick, MA, USA).

*Model 1: resonate-and-fire*

To investigate the effects of membrane potential oscillations on a neuron’s frequency transfer in the spiking regime, we adopted the Resonate-and-Fire model (as described in Erchova et al. 2004). The model’s subthreshold dynamics correspond to the damped oscillations of an RLC circuit and are given by a two-dimensional linear system:

$$C_m \frac{d}{dt} V_m(t) = I_{in}(t) + I_n(t) - I_{lk}(t) - I_L(t),$$

$$L \frac{d}{dt} I_L(t) = V_m(t) - V_0 - R_L I_L(t),$$

where

$$I_{lk}(t) = \frac{1}{R_m} (V_m(t) - V_0)$$

The membrane potential  $V_m$  is diverted from the resting potential  $V_0$  through injection of input current  $I_{in}(t)$  and the presence of neuronal noise  $I_n(t)$ . Depolarization is counteracted by both a leak current  $I_{lk}(t)$  (governed by membrane resistance  $R_m$  and capacitance  $C_m$ ) and an inductive current  $I_L(t)$ , mimicking the effects of a delayed rectifier potassium channel. Crossing of the constant voltage threshold  $V_{th}$  defines the occurrence of an action potential. In these cases,  $V_m$  is reset to a defined reset value  $V_r$  before the model progresses.

A subset of the model’s parameters were fixed, with  $V_0 = -70$  mV,  $V_{th} = -55$  mV and  $I_n$  consisting of Gaussian white noise with a standard deviation of 100 pA. The amplitude of  $I_{in}$  was set to either 100 or 200 pA, resulting in sub- or suprathreshold voltage excursions, respectively. To approximate the rMTF of ON1, the model’s remaining parameters were manually tuned to  $V_r = -60$  mV,  $R_m = 143.0$  M $\Omega$ ,  $C_m = 54.6$  pF,  $L = 860$  kH and  $R_L = 187.0$  M $\Omega$ . A detailed parameter scan was performed post hoc, illustrating the influence of inductance  $L$  and membrane time constant  $\tau_m = R_m C_m$  on the model’s frequency tuning. Simulations were performed at a temporal resolution of 200  $\mu$ s.

*Model 2: adaptive leaky integrate-and-fire*

The impact of spike-triggered adaptation and signal integration on a neuron’s frequency response was explored by implementing an adaptive Leaky Integrate-and-Fire model (Treves 1993). The subthreshold dynamics of the model are identical to the standard Leaky Integrate-and-Fire model and correspond to the characteristics of a low-pass RC circuit. They are given by

$$C_m \frac{d}{dt} V_m(t) = I_{in}(t) + I_n(t) - I_{lk}(t) - I_a(t).$$

In this model, a separate variable traces the progression of an adaptation current  $I_a$  which, by default, is zero. When the membrane potential crosses the firing threshold, the adaptation variable is incremented by a predefined value  $\Delta I_a$  and exponentially decays back to zero with time constant  $\tau_a$ :

$$\tau_a \frac{d}{dt} I_a(t) = I_a(t).$$

The adaptation current  $I_a$  acts as a spike-dependent rectifier, driving  $V_m$  away from  $V_{th}$ .

For the model to approximate the rMTF of ON1, a subset of parameters was manually tuned to  $V_r = -57$  mV,  $R_m = 59.0$  M $\Omega$ ,  $C_m = 59.6$  pF,  $\Delta I_a = 49.5$  pA and  $\tau_a = 9.2$  ms. The remaining parameters were identical to the ones used in the Resonate-and-Fire model. A subsequently applied parameter scan was used to illustrate the dependence of the model’s frequency transfer on both the adaptation time constant  $\tau_a$  and the membrane time constant  $\tau_m$ .

*Model 3: linear-nonlinear network*

A linear-nonlinear (LN) cascade (Schwartz et al. 2006; Clemens et al. 2012) was used to simulate the interactions of excitation and inhibition and their effect on frequency transfer in a small network :

$$r(t) = F[w_1(D_1 * s(t)) + w_2(D_2 * s(t - \Delta t))],$$

with

$$D_i * s(t) = \int_0^\infty D_i(\tau) s(t - \tau) d\tau,$$

$$D_i(x) = \frac{1}{\sqrt{2\pi} \cdot \sigma_i} \cdot e^{-\frac{x^2}{2\sigma_i^2}},$$

$$F(y) = \frac{a}{1 + e^{(y-y_0)/b}}.$$

The model consisted of two branches, both of which acted as linear low-pass filters by convolving identical copies of an input signal  $s$  with a Gaussian kernel  $D$  of width  $\sigma$ . The outputs of the two branches were combined in a weighted sum, where one branch was assigned an excitatory ( $w_1 > 0$ ) and the other one an inhibitory ( $w_2 < 0$ ) weight. Finally, a static nonlinearity  $F$  (a Boltzmann function with point of inflection  $y_0$ , saturation  $a$ , and width  $b$ ) was applied, yielding a rectified spike-rate estimate  $r$ . In summary, the model describes a neuron’s response to low-pass filtered copies of a stimulus received through excitatory and inhibitory afferents.

Taken alone, each branch acts as a low-pass filter. By means of small modifications in either the temporal or the spectral domain, the network as a whole can be equipped

with band-pass properties: In the first case (Fig. 6), the model's two branches had identical low-pass properties ( $\sigma_1 = \sigma_2$ ); the inhibitory branch, however, was given a delay  $\Delta t > 0$ . In the second case (Fig. 7), the delay was omitted ( $\Delta t = 0$ ). Instead, the cutoff frequency of the inhibitory low-pass filter was lowered relative to that of the excitatory branch ( $\sigma_1 > \sigma_2$ ).

Stimulus amplitude was set to 1. To achieve an approximation of ON1's rMTF through a delayed inhibition, the model's parameters were tuned to  $\sigma_1 = \sigma_2 = 3$  ms,  $w_1 = 0.88$ ,  $w_2 = -0.12$ ,  $\Delta t = 15$  ms,  $y_0 = 0.75$ ,  $a = 227$  Hz and  $b = 9$ . To fit the data with the model version based on spectral manipulation of the inhibitory component, parameters were tuned to  $\sigma_1 = 3$  ms,  $\sigma_2 = 6.5$  ms,  $w_1 = 0.84$ ,  $w_2 = -0.16$ ,  $\Delta t = 0$  ms,  $y_0 = 0.75$ ,  $a = 344$  Hz and  $b = 9$ .

## Results

### Modulation transfer functions of AN1, AN2 and ON1

In order to understand how the firing responses of neurons in the cricket auditory periphery depend on the AM frequency of the stimuli, we analyzed firing-rate resonances. We were inspired by a protocol known from the in-vitro characterization of subthreshold resonances, where neurons are stimulated with a sine wave whose frequency increases linearly with time (Gimbarzevsky et al. 1984). In the subthreshold voltage range, where the membrane potential varies in a graded manner, such a resonance analysis is straightforward. Subthreshold resonances reflect neuronal filtering where stimulus frequencies significantly larger than 0 Hz elicit responses with largest voltage amplitude. Such a resonance is readily captured by the membrane impedance, which can be directly calculated from the Fourier transform of the subthreshold voltage response (and the Fourier transform of the stimulus). Spiking responses, however, are not graded but pulsed. Hence, a few additional steps need to be taken into account for the analysis of a resonance based on firing rate. In this case, the resonance analysis can be based on a high-resolution peristimulus time histogram (PSTH), obtained from repeated presentations of a stimulus and a subsequent analysis of the time-resolved spectral content (described in more detail below). In addition, we chose acoustic stimulation (in contrast to current injection which is commonly used for subthreshold resonances). Analogously to the subthreshold case, the acoustic stimulus showed a sinusoidal amplitude modulation (AM) with a frequency increasing linearly over time. In other words, the stimuli consisted of swept-frequency amplitude modulated (SFAM) tones.

To experimentally identify firing-rate resonances in the AM frequency tuning, we obtained extracellular recordings from three auditory cell types in the prothoracic ganglion of

*G. bimaculatus*: the ascending neurons AN1 and AN2 that form the main input for auditory processes in the cricket brain (Boyan and Williams 1982; Schildberger 1984; Hennig 1988) as well as the local interneuron ON1 that inhibits the contralateral ascending neurons and its contralateral counterpart (Selverston et al. 1985; Horseman and Huber 1994).

The SFAM stimulation protocol is illustrated in Fig. 1a with a representative recording of neuron ON1. The stimulus consisted of a tone of 4.5 kHz carrier frequency with a sinusoidal amplitude modulation sweeping through frequencies of 1–100 Hz within 10 s. It covered an AM frequency range of particular relevance to the cricket: the ~25 Hz characteristic of the pulsed mating song of male conspecifics. The responses of ON1 to stimulus segments with a low modulation frequency were attenuated by spike frequency adaptation (Fig. 1b). Firing rates increased with modulation frequencies up to around 20 Hz (Fig. 1c), after which they started to decline again, with fewer spikes fitting the gradually contracting modulation periods of the stimulus (Fig. 1d). Eventually, at very high modulation frequencies, the cell decoupled from the stimulus and fired erratically at low overall rates (Fig. 1e). Altogether, the cell's response exhibited band-pass tuning in the range of the behaviorally relevant frequencies.

Spiking neuronal responses to acoustic stimulation with systematically varying AM frequencies allow for an analysis of both mean firing rates and stimulus-coupled firing. Both measures rely on a high-resolution PSTH. Because stimulation frequency increased linearly in time (SFAM protocol), the analysis of the spectral content of the PSTH yielded insights about frequency preference. Specifically, we extracted the so-called rate modulation transfer function (rMTF), and the temporal modulation transfer function (tMTF). The first represents the average firing rate as a function of stimulus frequency (Gerstein and Kiang 1960). The second captures the rate contribution of only those spikes that are temporally locked to the stimulus modulation. Graphically, these measures can be identified in a plot that depicts the frequency content of the firing response as a function of time, corresponding to a magnitude spectrogram (Fig. 2a). The rMTF corresponds to the amplitude along the horizontal line (Fig. 2a, marked in green), showing the dependence of the 0 Hz component (i.e., the mean) in time. The tMTF corresponds to the amplitude along the diagonal line (Fig. 2a, marked in blue). It characterizes the amplitude of the response at frequencies that linearly increase in time and hence, because of the design of the SFAM stimulus, correspond to the stimulation frequency. A cell's decoupling from a stimulus is therefore reflected in the divergence of the two measures—observed, for example, at high AM frequencies (Fig. 2b). Here, the cell is still firing (relatively high spectral magnitude of rMTF), but firing is decoupled from the frequency of the stimulus (relatively low spectral magnitude of

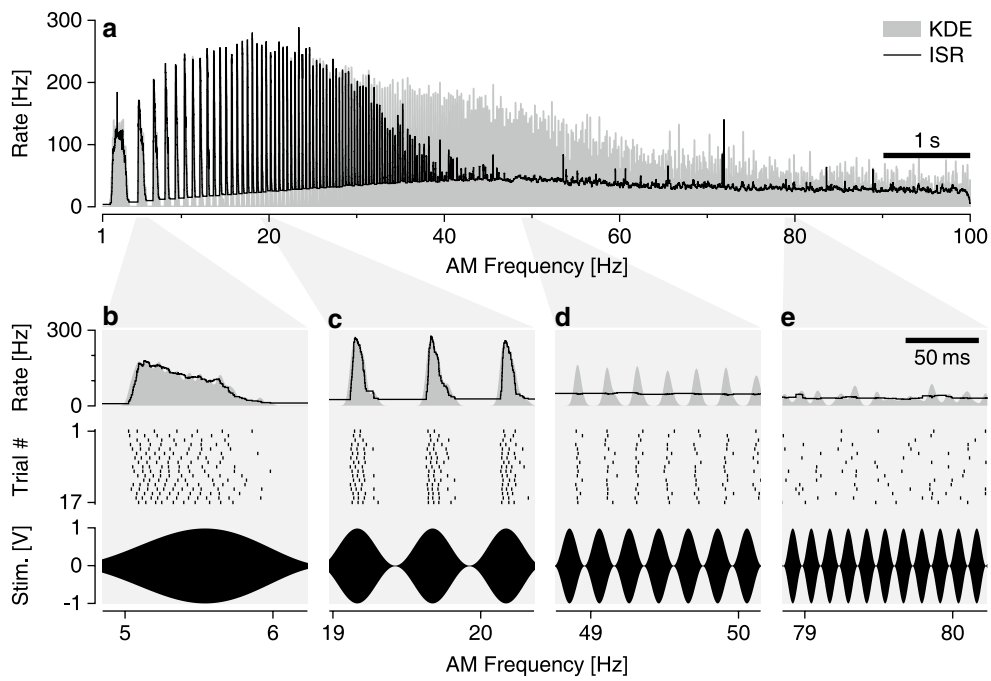


**Fig. 1** Exemplary response of ON1 to a 10 s SFAM stimulus rising in modulation frequency from 1 to 100 Hz (80 dB SPL, 4.5 kHz carrier frequency). **a** Kernel density estimation (KDE, gray) overlaid with average instantaneous spike rate (ISR, black) across 17 trials. **b–e** Selected periods from panel a showing (from top to bottom)

KDE (gray) overlaid with average ISR (black), a spike raster plot, and the respective section of the acoustic stimulus. **b** Spike-frequency adaptation erodes the response. **c** High firing rates, several spikes per stimulus period. **d** Stimulus-locked firing at low overall firing rates. **e** Desynchronized firing at low firing rates

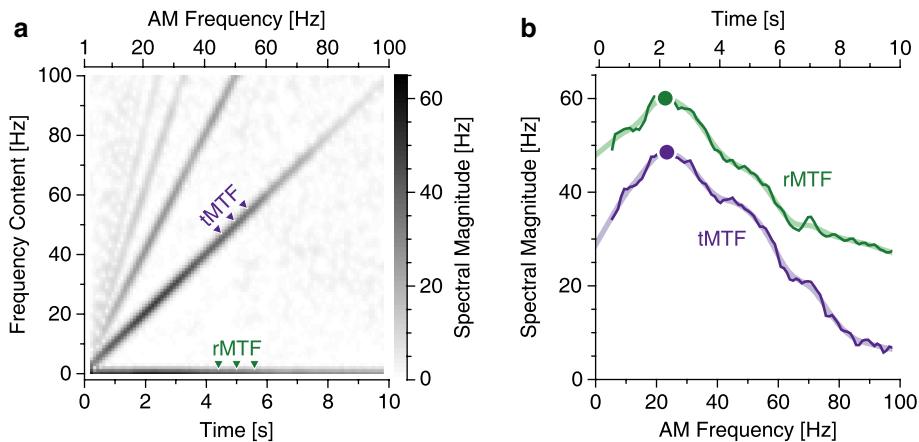


**Fig. 2** Modulation transfer functions. **a** Magnitude spectrogram of a cell's spiking response to an SFAM stimulus (average across 17 repetitions, same data as in Fig. 1). Because modulation frequency changes linearly with time, modulation transfer functions are readily obtained from spectral cross-sections: the rate modulation transfer function (rMTF) is identified by the spectrogram's DC component, indicating average firing rate as a function of modulation frequency. The temporal modulation transfer function (tMTF) corresponds to

the spectral cross-section along the envelope's rising fundamental frequency; it represents the absolute rate contribution of stimulus locked spikes. The bands to the left of the tMTF represent harmonics in the spiking response. **b** rMTF and tMTF from the spectrogram. To ease the automated detection of transfer peaks in individual recordings, data was smoothed with cubic smoothing splines (broad lines). Filled circles indicate peak frequencies: 23.0 Hz (rMTF) and 23.5 Hz (tMTF);  $Q$  values 1.25 and 1.69, respectively

tMTF). To facilitate the algorithmic detection and characterization of transfer peaks in individual recordings, the respective transfer functions were fitted with cubic smoothing splines.

Figure 3a–d shows the modulation transfer functions of AN1, AN2 and ON1, averaged across all recordings. AN1 exhibited a relatively flat tMTF with no indications for sharp

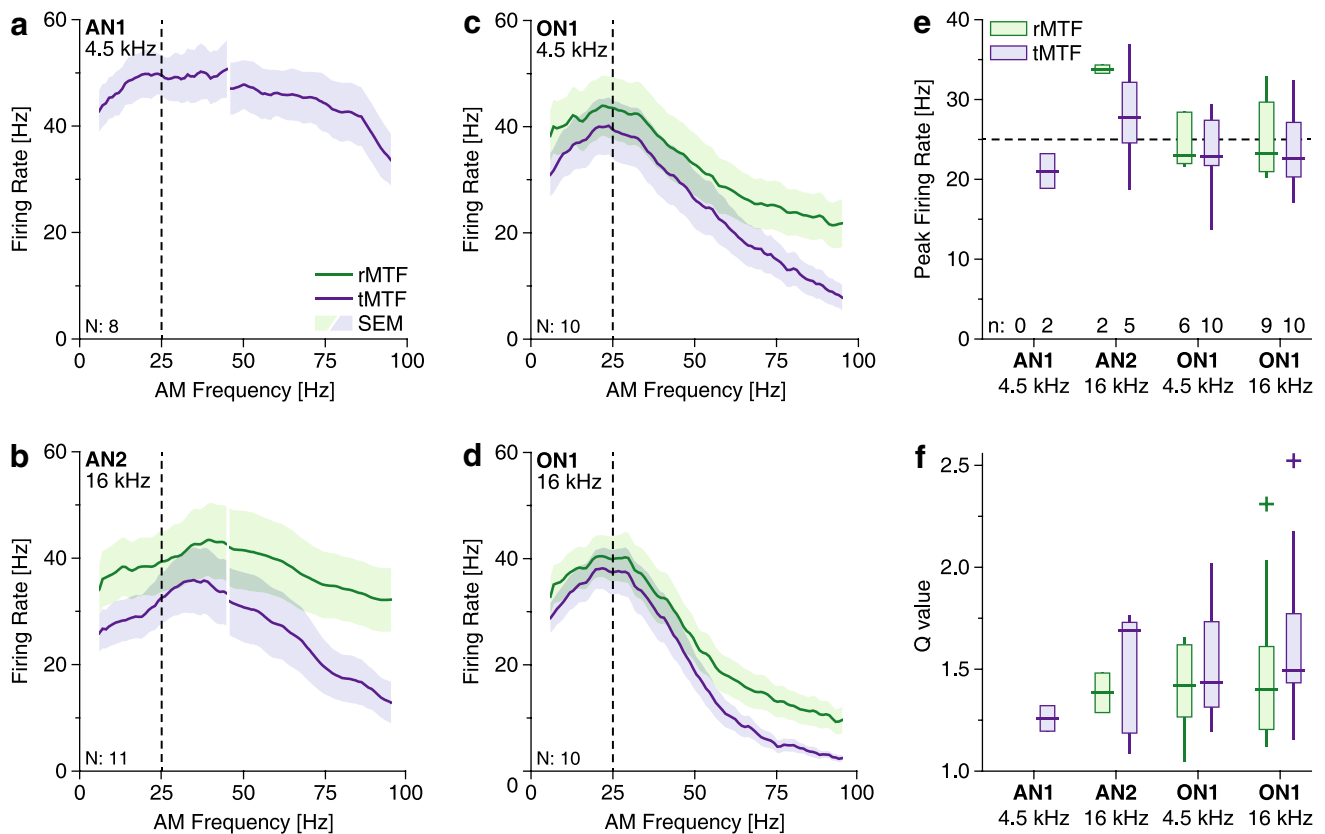


**Fig. 3** Summarized results of electrophysiological experiments. Stimulation was performed at 4.5 or 16 kHz carrier frequency, depending on cell type. **a–d** Mean modulation transfer functions (MTFs) by cell type across all recordings. Panels **a** and **b** comprise two sets of stimuli with different ranges of AM frequencies, hence the apparent seam in the respective MTFs. *N* denotes the number of

recordings. **e** peak frequencies for detected peaks in MTFs of individual recordings. The *dashed lines* indicate the 25 Hz pulse frequency typical for songs of *G. bimaculatus*. *n* denotes the number of individual recordings with detected peaks. **f** Corresponding *Q* values with values above 1 indicating pronounced resonant peaks. Outliers are marked with *crosses*

band-pass tuning (Fig. 3a). Due to a relatively high rate of false-positive spike events often evident in hook electrode recordings of AN1 (Faulkes and Pollack 2000), its rMTF could not be derived reliably and was hence omitted. While false positive spike events do add to the noise floor of the mean rate, they are not phase-locked to the stimulus and thus have no impact on the tMTF. AN2 showed clear firing-rate resonances, peaking at modulation frequencies of around 30–40 Hz (Fig. 3b). Its rMTF had a slightly increased peak frequency with respect to its tMTF. The two MTFs of ON1 exhibited a more pronounced drop-off towards higher modulation frequencies; for both measures, distinct band-pass tuning was observed, with peak frequencies at ~25 Hz (Fig. 3c, d). Stimuli with a high carrier frequency resulted in a sharper tuning than those with a low carrier frequency, which is different to previous findings for *T. oceanicus* based on comparable measures (cf. Marsat and Pollack 2004).

In addition to the average MTFs, we also analyzed the statistics across recordings: transfer peaks detected in individual recordings were characterized by their respective

peak frequency and *Q* values, as summarized in Fig. 3e, f and Table 1. The *Q* value indicates how pronounced a resonance is. We used a definition of the *Q* value often encountered in the analysis of subthreshold resonance: the ratio between the amplitude at the peak and the amplitude at 0 Hz. This ratio equals one for low-pass characteristics (cases of no resonance) and is larger than one in cases of resonance (see Fig. 3f). Please note that various other, though related measures termed *Q* values are used in different fields to quantify the “quality” of a resonance. By its definition, the *Q* value used here characterizes the low-frequency drop-off of a filter—it does not capture differences in the high-frequency drop-off.

#### Model: different means to obtain a neuronal band-pass filter

Results from our experiments suggest that both AN2 and ON1 are tuned to behaviorally relevant stimulus frequencies. In contrast to approaches like the ZAP protocol, which

**Table 1** Detected peaks in individual modulation transfer functions

Type	$f_c$ (kHz)	$N$	rMTF			tMTF		
			$n_p$	$\tilde{f}_c$ (Hz)	$\tilde{Q}$	$n_p$	$\tilde{f}_c$ (Hz)	$\tilde{Q}$
AN1	4.5	8	0	–	–	2	21.0	1.26
AN2	16.0	11	2	33.8	1.38	5	27.7	1.69
ON1	4.5	10	6	22.9	1.42	10	22.8	1.44
ON1	16.0	10	9	23.2	1.40	10	22.6	1.49

$f_c$  denotes the carrier frequency used for stimulation,  $N$  the number of recordings,  $n_p$  the number of recordings with detected transfer peaks.  $\tilde{f}_c$  and  $\tilde{Q}$  correspond to the median peak frequency and median  $Q$  value of the respective peaks

is used for the characterization of subthreshold frequency transfer (cf. Gimbarzevsky et al. 1984), our approach focusses on firing-rate resonances. Moreover, stimulation is acoustic and does therefore not drive the recorded cells directly: the acoustic stimuli are first processed by receptors and other neurons in the local network, so that the response characteristics are shaped both by the recorded neurons themselves and by upstream neurons. The observed firing-rate resonances could hence be based on both cell-intrinsic and network-based mechanisms. While we cannot identify the physiological mechanisms shaping the resonance based on our experiments, we use mathematical models to show that three generic and well-established principles are compatible with the observed firing-rate resonance: (1) subthreshold resonances, (2) spike-frequency adaptation, and (3) an interplay of excitation and inhibition. We tuned these models to match the average rMTF of ON1 (Fig. 3f,  $f_p = 23.9$  Hz,  $Q = 1.34$ ), as this cell type indicated the most pronounced tuning during our electrophysiological experiments, and the given measure is suited for investigating a system that relies on a rate-code (cf. Schildberger 1984; Kostarakos and Hedwig 2012).

In the first model, firing-rate resonances were induced cell-intrinsically through subthreshold resonances of the membrane potential. Subthreshold resonances have been well characterized in many cell types (for a review, see Hutcheon and Yarom 2000) and give rise to band-pass filtering in the subthreshold range of membrane potentials. These filter properties can also carry over to the firing regime (Schreiber et al. 2004; Engel et al. 2008; Izhikevich 2001; Schreiber et al. 2009) and shape a firing-rate resonance (Richardson et al. 2003). We implemented a Resonate-and-Fire model (Izhikevich 2001), where excursions of the membrane potential are counteracted by an inductive current. The model’s resonant dynamics lead to an initial voltage overshoot in response to a subthreshold current pulse which translates into a corresponding initial overshoot of the firing rate in the suprathreshold regime (Fig. 4a, b). Accordingly, resonances manifested themselves in both the sub- and suprathreshold frequency transfer (Fig. 4c,

d). By manually tuning the parameters (see "Materials and methods"), the model displayed a firing-rate resonance at 23.9 Hz with a  $Q$  value of 1.34, closely resembling the rMTF of ON1. For frequencies above  $\sim 50$  Hz, however, the model’s frequency transfer diverged from the experimentally obtained data. For completeness, we note that this discrepancy stemmed from the limited number of model parameters, preventing an independent control of low- and high-frequency filter characteristics.

The characteristics of the firing-rate resonance, like the peak frequency and  $Q$  value, depended on the model’s parameters. To illustrate the robustness of tuning, these values are shown as a function of the parameters for inductance  $L$  and membrane time constant  $\tau_m$  (Fig. 4e, f). Both parameters correlated positively with the peak frequency and the  $Q$  value of the model’s firing-rate resonance, but to different degrees: while the membrane time constant had the bigger influence on the peak frequency, the  $Q$  value could be controlled by means of the inductance.

The second model relies on the effect of adaptation, a universal phenomenon in neuronal systems that may be caused by a variety of mechanisms. Some of these mechanisms effectively depend on the occurrence of action potentials, as the adaptation currents are caused by ionic conductances that activate only at weakly negative or even positive membrane potentials which require large depolarizing voltage excursions. Such conductances can, for example, comprise M-type or mAHP-type currents with high activation thresholds (Benda and Herz 2003). The adapting Leaky Integrate-and-Fire neuron (Treves 1993) allows to implement an adaptation-based firing-rate resonance by combining high-pass properties of spike-triggered adaptation with low-pass properties of the non-resonant subthreshold voltage dynamics (Fig. 5a, b). Here, the adaptation current only depended on the occurrence of spikes and, in contrast to the model described above, the voltage dynamics did not exhibit band-pass properties in the subthreshold regime (Fig. 5c). In the spiking regime, however, the adaptation current  $I_a$  added a high-pass component to the response, leading to a firing-rate resonance (Fig. 5d).

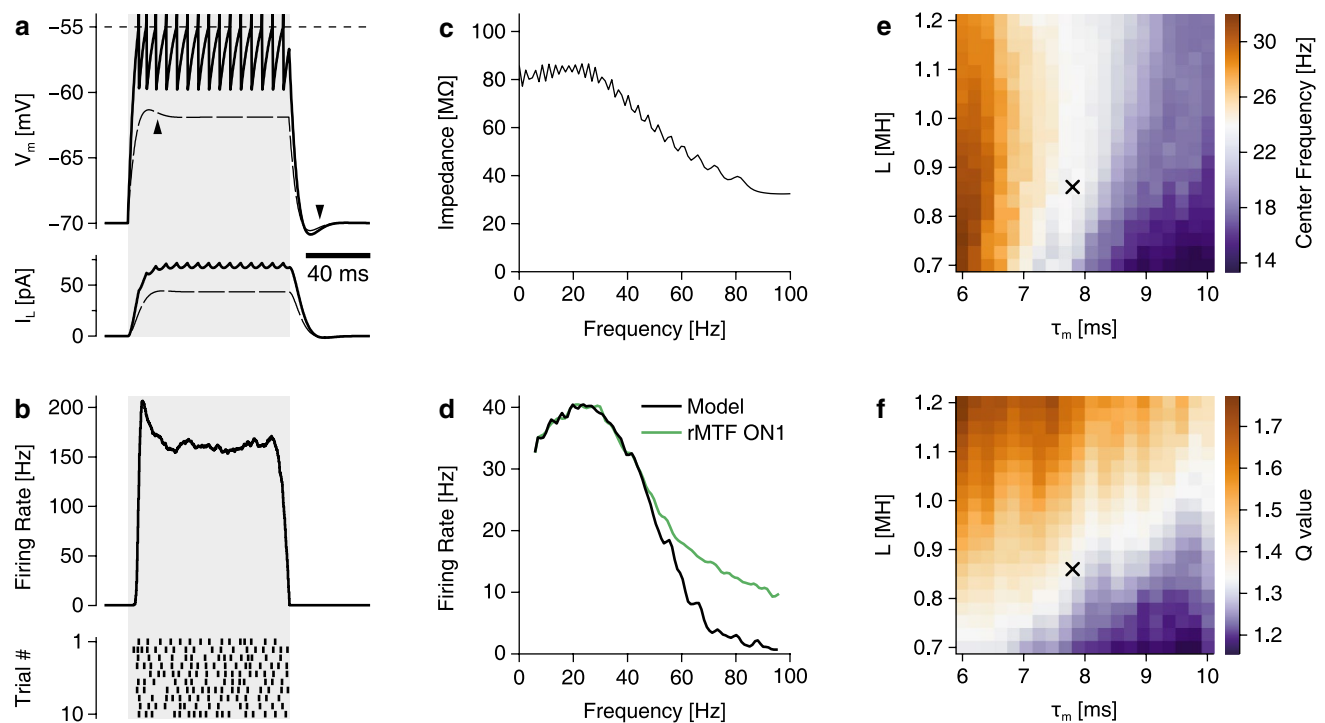


**Fig. 4** Resonate-and-Fire model. **a** Subthreshold (*dashed*) and suprathreshold (*solid*) responses to current pulses of either 100 or 200 pA amplitude and 100 ms duration (*gray*). In this panel, the noise current was omitted for clarity. Note the damped voltage oscillations after onset and offset of the current (*arrows*). **b** Firing rate profile in response to a 200 pA pulse, 20 repetitions. Instantaneous spike rate (*top*) and exemplary spike raster plot (*bottom*). **c** The subthreshold

impedance amplitude profile (ZAP) displayed a weak resonance peak at 19.3 Hz with a  $Q$  value of 1.04. **d** Suprathreshold frequency transfer, 50 repetitions, peaking at 23.9 Hz with a  $Q$  value of 1.34. **e, f** A parameter scan serves to illustrate the impact of membrane time constant  $\tau_m$  and inductance  $L$  on peak frequency and  $Q$  value. The parameter combination used in a–d is marked by a *cross*

By tuning the model's parameters we were able to obtain a peak frequency of 23.6 Hz with a  $Q$  value of 1.34, closely matching the data obtained for ON1. We again applied an exemplary parameter scan to illustrate the influence of individual parameters on the model's transfer function. While the peak frequency of the firing-rate resonance was strongly influenced by the membrane time constant  $\tau_m$ , the adaptation time constant  $\tau_a$  had only little effect (Fig. 5e). Nevertheless,  $\tau_a$  exhibited a clear influence on the  $Q$  value of the firing-rate resonance (Fig. 5f).

Computation within the cricket's auditory system is not limited to intracellular mechanisms. Despite its size, the prothoracic system has an interesting topology that includes both excitatory and inhibitory elements (Wohlers and Huber 1982). ON1 neurons, in particular, receive excitatory inputs from the receptor populations and inhibitory inputs from its contralateral counterpart (cf. Wiese and Eilts 1985; removal of the contralateral inhibition in *T. oceanicus*, however, did not affect the information tuning: Marsat and Pollack 2004). We hence implemented a simple model of the local network based on a linear-nonlinear (LN) cascade and investigated the formation of firing-rate resonances based on the interactions of excitatory and inhibitory network components.

Specifically, we analyzed two versions of the model, equivalent to different physiological implementations. Both provide a firing rate estimate by computing the weighted sum of two low-pass filtered copies of the stimulus—one of them “excitatory” (additive), the other one “inhibitory” (subtractive)—and applying a rectifying Boltzmann non-linearity (Figs. 6, 7). Resonances were introduced through parameters of the inhibition—either in time or in the frequency domain: In the first case, a temporal delay  $\Delta t$  was added to the inhibitory branch (Fig. 6a). While this did not affect the two branches' individual frequency transfer (Fig. 6c), their combined output showed a clear resonance which we tuned to a peak frequency of 23.8 Hz and a  $Q$  value of 1.35 (Fig. 6d). In the second case, the low-pass filter of the inhibitory branch was set to a lower cutoff frequency than that of the excitatory branch (Fig. 7a). After tuning the respective parameters (see “Materials and methods”), the two filters' frequency transfers (Fig. 7c) combined to an accurate approximation of the rMTF of ON1, with a peak frequency of 23.8 Hz and a  $Q$  value of 1.37.

Overall, all three model types produced a good quantitative match to the experimental data, despite differences in the underlying biophysical mechanisms (subthreshold

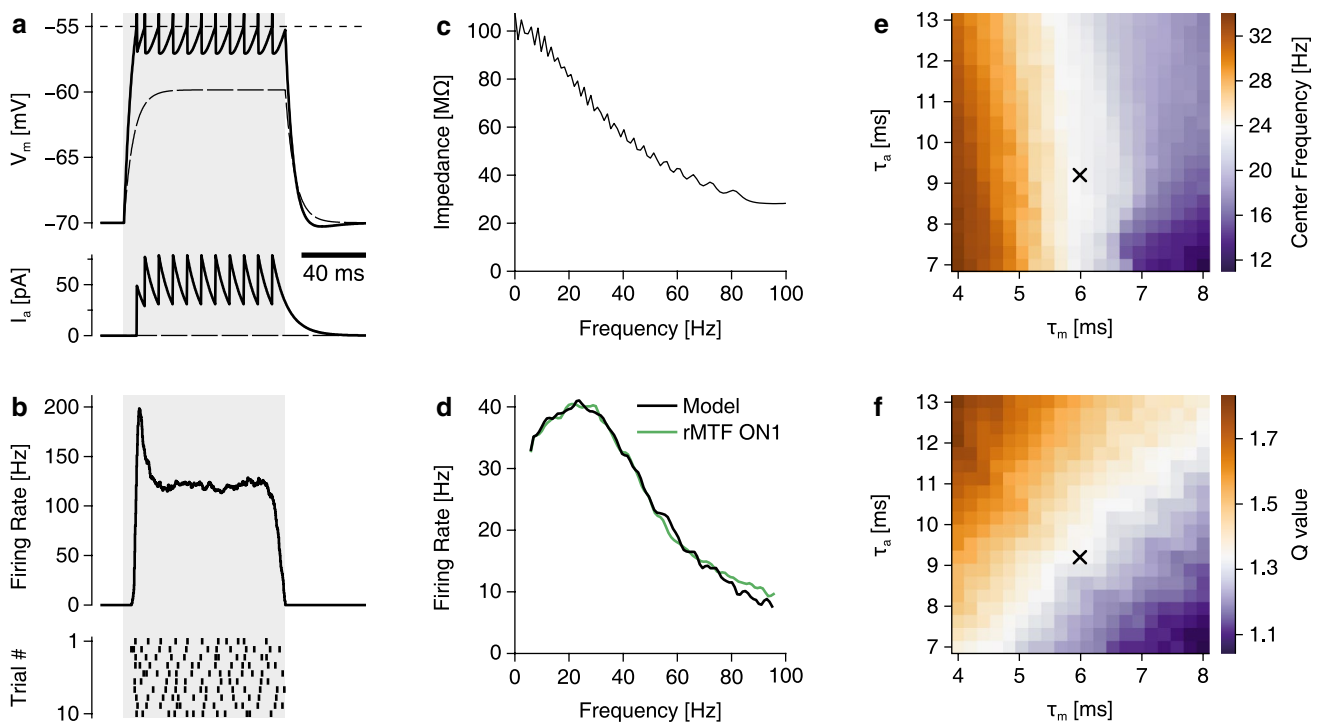


**Fig. 5** Adaptive Leaky Integrate-and-Fire Model. **a** Subthreshold (dashed) and suprathreshold (solid) responses to current pulses of either 100 or 200 pA amplitude and 100 ms duration (gray). In this panel, the noise current was omitted for clarity. The adaptation current  $I_a$  is increased with each spike and decays in an exponential manner. **b** Firing rate profile in response to a 200 pA pulse with added noise current, 20 repetitions. Instantaneous spike rate (top) and

exemplary spike raster plot (bottom). **c** The subthreshold impedance amplitude profile (ZAP) displayed no resonance. **d** Suprathreshold frequency transfer, 50 repetitions, peaking at 23.6 Hz with a  $Q$  value of 1.34. **e, f** A parameter scan serves to illustrate the impact of membrane time constant  $\tau_m$  and adaptation time constant  $\tau_a$  on peak frequency and  $Q$  value. The parameter combination used in a–d is marked by a cross

resonance, spike-frequency adaptation, and properties of the inhibition).

### Discussion

Using an efficient experimental protocol, we quantified firing-rate resonances in several peripheral auditory neurons of the cricket *G. bimaculatus* that are tuned to behaviorally relevant frequencies. We further demonstrated that our experimental findings can be consistently reproduced by three different mathematical neuron models which rely on single-cell mechanisms (subthreshold resonance or spike-triggered adaptation) or specific properties of inhibition in the local network. In general, the analyzed mechanisms are interesting candidates for firing-rate resonances beyond the cricket auditory system.

### Experimental protocol

To assess an auditory neuron’s frequency transfer at the level of firing rates, we conceived of a straightforward protocol that uses acoustic stimuli sweeping through a range

of modulation frequencies (Figs. 1, 2). Our approach draws inspiration from the ZAP protocol (Gimbarzevsky et al. 1984; Hutcheon and Yarom 2000; Schreiber et al. 2004), used to assess the frequency dependence of subthreshold voltage responses in single cells. In contrast to the latter approach, however, we here characterize a neuron’s suprathreshold firing rate responses to cell-external stimuli. Thus, the observed frequency characteristics are not shaped by the recorded cell’s subthreshold properties alone, but also by properties of its spike generating mechanism and upstream elements (including the mechanical properties of the tympanum, sensory transduction processes and properties of the receptor neurons). Although a number of protocols have been used to assess firing-rate resonances in auditory networks, the SFAM protocol has general advantages with relevance to our study: First, it quantifies both mean and stimulus-locked firing rates (rate and temporal modulation transfer functions). Second, SFAM stimuli can assess a broad range of modulation frequencies within a short time, thus providing a better consistency in recording conditions and an overall reduced recording time, when compared to stimuli with a constant modulation frequency (Farris et al. 2004; Schildberger 1984; Kostarakos and Hedwig 2012).

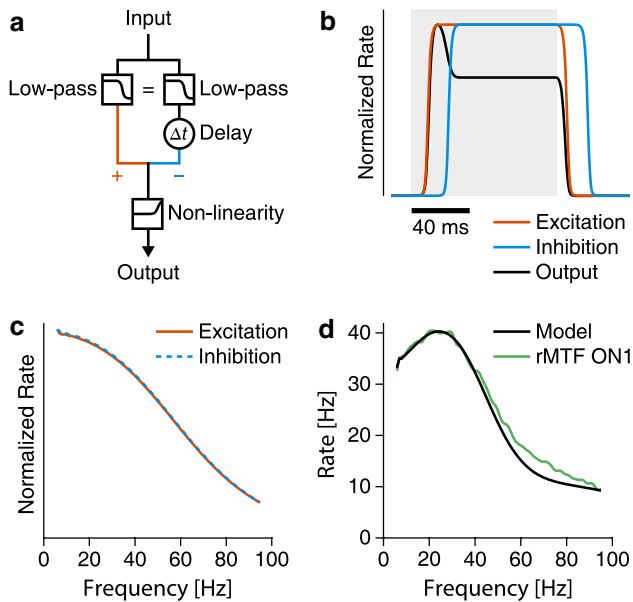


**Fig. 6** LN Network Model, variant 1. **a** Schematic. The input was processed in two parallel branches, one excitatory (+) and one inhibitory (−). In both branches, the signal was low-pass filtered with identical cutoff frequencies. In the inhibitory branch, however, the signal was delayed by  $\Delta t$ . The weighted sum of the two branches' output was passed through a sigmoidal non-linearity to obtain a firing rate estimate. **b** Response of the model and its components to a pulse stimulus (gray). Note the onset peak of the model's output. **c** Identical frequency transfer of the model's excitatory and inhibitory branches. **d** Frequency transfer of the model compared to data measured during experiments

Third, while they lack a chirp component, SFAM stimuli involve a pulse-like amplitude modulation and are thus still similar to the cricket's natural song (refer to Hennig 2009 for the attractiveness of continuous pulse trains).

### Firing-rate resonances of neurons and behavioral relevance

The auditory pathway of the cricket is a dedicated system designed to detect and localize two classes of objects: mating partners and predators, most prominently bats. In line with these tasks, peripheral frequency filtering and object categorization is well known (Wohlers and Huber 1978; Wytenbach et al. 1996; Hildebrandt 2014). At the network level of the peripheral auditory system of the cricket, AN1 and AN2 represent the two channels of information transmission associated with such a categorical perception, as given by their differential tuning for low and high carrier frequencies (Wohlers and Huber 1978; Hennig 1988) and their ability to modulate behavior (for AN1: Schildberger and Hörner 1988; for AN2: Nolen and Hoy 1984; Marsat and Pollack 2006). The function of ON1 is usually attributed to localization (Selverston et al. 1985). As ON1

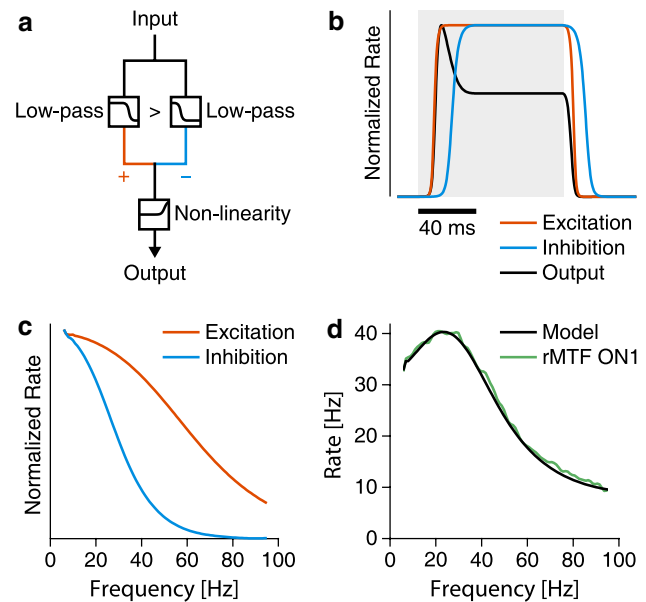


**Fig. 7** LN Network Model, variant 2. **a** Schematic. Like in the previous model, the input is simultaneously processed by an excitatory (+) and an inhibitory (−) branch, both of which acted as low-pass filters. The cutoff frequency of the inhibitory branch was lower than that of the excitatory branch. The weighted sum of the two branches' output was passed through a sigmoidal non-linearity to obtain a firing rate estimate. **b** Response of the model and its components to a pulse stimulus (gray). **c** Frequency transfer of the model's excitatory and inhibitory branches. **d** Frequency transfer of the model compared to data measured during experiments

exhibits wide carrier tuning, it affects both transmission channels.

To adequately stimulate the low frequency channel of *G. bimaculatus*, we chose a carrier frequency of 4.5 kHz, corresponding to the fundamental carrier frequency of the species' calling song (Doherty 1985) and the characteristic frequency of AN1 (Fig. 2 in Schildberger 1984). The transfer function of AN1 did not exhibit a clear tuning to the 25 Hz modulation rate of the calling song but was rather broadly tuned (Fig. 3a; Table 1) in line with studies on other cricket species (*T. oceanicus*: Benda and Hennig 2008, *G. assimilis*: Pollack and Kim 2013). On the level of information rate, however, such a tuning has previously been demonstrated (*T. oceanicus*: Marsat and Pollack 2005). Clear rate coding for conspecific pulse patterns apparently only manifests at higher processing stages as evidenced by the observed broad tuning of AN1 and the hierarchical tuning of brain neurons (Schildberger 1984; Kostarakos and Hedwig 2012). The temporal tuning of ON1 at low carrier frequencies is well known, although its primary role is usually seen in the context of contrast enhancement of binaural localization cues. Early reports even proposed oscillatory properties for ON1 (Wiese and Eilts 1985), but low- and band-pass selectivity was also described—albeit

by different measures (instantaneous spike rate: Nabatiyan et al. 2003, information rate: Marsat and Pollack 2004). The observation of ON1's temporal tuning to the pulse rate of the conspecific calling song (Tunstall and Pollack 2005) corroborates its role in a dedicated network and likely accounts for the firing-rate resonances observed here (Fig. 3c).

The high frequency channel was stimulated with a carrier frequency of 16 kHz, based on the characteristic frequency of AN2 (Fig. 2 in Schildberger 1984). In contrast to AN1, both AN2 and ON1 display a fairly broad carrier tuning (Wohlers and Huber 1982) which covers both the low power harmonics of cricket's calling song (Nolen and Hoy 1986) and courtship song (Libersat et al. 1994) as well as the ultrasound cries of predatory bats (Schnitzler and Kalko 2001). In the high frequency channel the transfer functions of ON1 and AN2 revealed temporal selectivity between 25 and 40 Hz, respectively (Fig. 3b, d; cf. Marsat and Pollack 2004, 2005). Although burst coding of AN2 is known to mediate an evasive response in flying crickets (Marsat and Pollack 2006), the firing-rate resonance within the frequency channel that is attributed to bat detection may also contribute to an adaptive response of flying crickets: For insects different evasive strategies upon bat detection are well known (Roeder 1962) and may at least in part be mediated by a filter for high pulse rates (moth: Boyan and Fullard 1988; mantid: Triplehorn et al. 2008; Yager 2012). To that effect, the AN2 could play a role in mediating a tactical switch in the cricket's evasive behavior (Fullard et al. 2005).

### Mathematical neuron models

Resonances of *subthreshold* voltage responses have been extensively discussed in the literature (see Hutcheon and Yarom 2000 for a review). For the transfer of information between neurons, however, the suprathreshold (i.e., spiking) response is relevant, because in many networks neurons are coupled via spikes rather than subthreshold membrane potentials. The mechanisms that shape firing-rate resonances, however, are diverse. While the mathematical models discussed in this study have individually been presented before, we here provide a comparative analysis showing that all three conceptually different models, based on either single-cell or network based phenomena, are equally effective in reproducing and explaining the experimentally observed firing-rate resonances. These mechanisms are likely to underly firing-rate resonances in many other systems and we hope to encourage the use of the corresponding mathematical models beyond the auditory neurons at hand. Accordingly, the number of model parameters was deliberately kept as low as possible, emphasizing the working principles and the robustness of the reviewed mechanisms.

In the first model—an implementation of the Resonate-and-Fire model as in Erchova et al. 2004—firing-rate resonances emerged from a band-pass in the subthreshold membrane impedance (Fig. 4). Web et al. 2007 demonstrated that such a mechanism could explain phonotactic preference functions of bushcrickets by fitting a similar model (Izhikevich 2001) to behavioral data of *Tettigonia cantans*. Subthreshold resonances do not have to be particularly strong to produce a considerable effect on firing rates: a subthreshold impedance with a  $Q$  value of 1.04 was sufficient in matching the experimentally observed firing-rate resonance (Fig. 4c). Note that this observation is similar to what has been termed the iceberg effect in the visual system, where subthreshold responses have been shown to exhibit broader selectivity than firing responses (e.g., Rose and Blakemore 1974). In the model at hand, the mild peak in the subthreshold membrane impedance translates to a sharper peak in the frequency dependence of the firing rate because of the threshold nonlinearity. Interestingly, this simple mechanism for sharpening the resonance does not require additional processes that exhibit band-pass filter properties on their own—a simple threshold nonlinearity suffices. One may speculate that in analogy to such an iceberg effect on the cellular level, a cellular firing-rate resonance in the periphery may result in an even stronger frequency selectivity in neurons of the cricket brain when combined with suitable nonlinearities at subsequent processing stages. Such nonlinearities may involve additional band-pass filters, but they do not have to. Simple threshold-like nonlinearities and hence simple non-resonant neurons with a firing threshold at sufficiently high voltages (that pick up only the frequencies with largest response) could, in principle, be sufficient to produce a high frequency selectivity in the brain, as long as a modest resonance is present in the periphery. Note that there currently is no evidence in support of this effect in the cricket auditory system. Nevertheless, it is worth pointing out that, from a more general perspective of nervous system design, weak resonances can be sufficient to shape stronger resonances in downstream neurons when combined with nonlinearities. Returning to subthreshold resonances, direct evidence for such a mechanism in the cricket auditory periphery would be provided by intracellular recordings—previous studies involving this technique, however, did so far not indicate subthreshold resonances (Wohlers and Huber 1978, 1982; Selverston et al. 1985). Evidence for network based over intrinsic mechanisms (in the recorded cells) was provided for *T. oceanicus* by (Sabourin and Pollack 2010), as information tuning was essentially unchanged when spikes and, presumably, most or all subthreshold conductances, were suppressed by strong hyperpolarization.

In the second model, a variation of the Leaky Integrate-and-Fire model, subthreshold voltage dynamics were non-resonant (Fig. 5). In the suprathreshold regime, however,

a spike-triggered, slowly decaying adaptation current provided suppression of low frequencies (Benda and Hennig 2008). Here, as in the first model, parameters affected different aspects of the transfer function, enabling us to independently tune peak frequency and  $Q$  value (Fig. 5e, f). The resonance-generating mechanism is very similar to the Resonate-and-Fire model: Potassium channels, for instance, could underlie the resonances in both models, but their activation curves would be shifted. For activation of potassium channels at lower voltages, a subthreshold resonance becomes evident. If, however, the potassium channel activation curve is shifted to more depolarizing voltages (so that voltage elevations required for activation are only reached during a spike), resonance manifests itself only in the supra-, but not the subthreshold range. Subthreshold resonance and spike-frequency adaptation are thus mechanistically and biophysically highly related phenomena.

In the third model, band-pass filtering relied on the combination of low-pass excitation and low-pass inhibition in a network of linear-nonlinear (LN) neurons. In one version of the model, high-pass properties were introduced by a temporal delay in the network's inhibitory branch (cf. Bürck and van Hemmen 2009): input components shorter than this delay fully contributed to the rectified output rate; longer ones were attenuated by inhibition (Fig. 6). In an alternative version of the model, band-pass filtering arose from differences in the spectral structure of the excitatory and inhibitory signal (Fig. 7). Inhibition specifically reduced low frequency components of a more broadly-tuned excitation. Both models reproduced the firing-rate resonance well. Nevertheless, in the first version of the model delays on the order of  $\sim 15$  ms were needed. While such long inhibitory delays are generally feasible they seem unlikely for a system as small as the cricket's prothoracic auditory network.

Please note that, in general, all mechanisms discussed here need not produce an exceedingly strong bandpass-tuning. When they are part of a distributed filtering cascade, the transfer characteristics of several serially arranged filter elements of moderate individual strength could result in a much stronger tuning.

## Conclusion

Using an efficient stimulus protocol to record neuronal responses to a wide range of stimulus frequencies, we quantified firing-rate resonances in the peripheral auditory system of crickets. Most neurons expressed clear bandpass tuning, indicating that the small nervous system of the cricket focuses its coding capacity on behaviorally-relevant cues. Contrary to our initial expectations, AN1 did not yield a clear bandpass tuning, contradicting the idea of strong filtering for calling song signals in the periphery (Nabatiyan

et al. 2003; Pollack and Kim 2013). Evidently, information about song patterns, for which pulse rate is a salient cue, is extracted by a dedicated circuit in the cricket's brain. However, information about direction across both relevant frequency ranges (ON1; Selverston et al. 1985; Horseman and Huber 1994) and predator signals in the ultrasonic range (AN2; Nolen and Hoy 1984) appear to be represented in a more selective manner at the prothoracic level of processing.

Our models show that several ubiquitous neuronal principles are equally effective in producing bandpass properties: subthreshold resonances, spike-triggered adaptation, as well as an interplay of excitation and inhibition. In this context, distinct neuronal mechanisms can fit a common conceptual framework: single-cell and network models share a negative feedback component, implemented either through ion channels (for subthreshold resonance and spike-frequency adaptation) or at the level of synaptic transmission (Urdapilleta and Samengo 2015). Feedback is a common theme in sensory processing; resonance in the response of individual neurons is a direct consequence. The firing-rate resonances observed in the experimental data are most likely produced by an interplay of several of these mechanisms (cf. Rössert et al. 2011)—future studies will identify the contribution of individual mechanisms by quantifying the subthreshold impedance, firing rate adaptation, or the timing of inhibitory versus excitatory inputs.

**Acknowledgments** This work was funded by grants from the Federal Ministry of Education and Research, Germany (01GQ1001A, 01GQ0901, 01GQ0972, 01GQ1403) and the Deutsche Forschungsgemeinschaft (SFB618, GRK1589/1). We are grateful to Wei Wu for valuable discussion. We thank Manuel Gersbacher, Michael Reichert, Frederic Römschied, Jan-Hendrik Schleimer and Vanessa Stempel for helpful comments on the manuscript.

## Compliance with ethical standards

**Conflict of interest** The authors declare that they have no conflict of interest.

**Ethical standard** The experiments conducted in this study comply with the current laws of Germany and the *Principles of animal care*, publication No. 86–23, revised 1985 of the National Institute of Health.

## References

- Barlow HB (1961) Possible principles underlying the transformation of sensory messages. In: Rosenblith WA (ed) *Sensory communication*. MIT Press, Cambridge, pp 217–234
- Benda J, Hennig RM (2008) Spike-frequency adaptation generates intensity invariance in a primary auditory interneuron. *J Comput Neurosci* 24(2):113–136
- Benda J, Herz AVM (2003) A universal model for spike-frequency adaptation. *Neural Comput* 15(11):2523–2564
- Bennet-Clark HC (1989) Songs and the physics of sound production. In: Huber F, Moore TE, Loher W (eds) *Cricket behavior and neurobiology*. Cornell UP, Ithaca, pp 227–261

- Borst A, Haag J (1996) The intrinsic electrophysiological characteristics of fly lobula plate tangential cells: I. Passive membrane properties. *J Comput Neurosci* 3(4):313–336
- Borst A, Theunissen FE (1999) Information theory and neural coding. *Nat Neurosci* 2(11):947–957
- Boyan GS, Fullard JH (1988) Information processing at a central synapse suggests a noise filter in the auditory pathway of the noctuid moth. *J Comp Physiol A* 164(2):251–258
- Boyan GS, Williams JLD (1982) Auditory neurones in the brain of the cricket *Gryllus bimaculatus* (De Geer): ascending interneurons. *J Insect Physiol* 28(6):493–501
- Bürck M, van Hemmen JL (2009) Neuronal identification of signal periodicity by balanced inhibition. *Biol Cybern* 100(4):261–270
- Bush SL, Schul J (2006) Pulse-rate recognition in an insect: evidence of a role for oscillatory neurons. *J Comp Physiol A* 192(2):113–121
- Cariani PA (2001) Specialist and generalist strategies in sensory evolution. *Artif Life* 7(2):211–214
- Clemens J, Wohlgenuth S, Ronacher B (2012) Nonlinear computations underlying temporal and population sparseness in the auditory system of the grasshopper. *J Neurosci* 32(29):10053–10062
- Doherty JA (1985) Temperature coupling and 'trade-off' phenomena in the acoustic communication system of the cricket, *Gryllus bimaculatus* De Geer (Gryllidae). *J Exp Biol* 114(1):17–35
- Eggermont JJ, Wang X (2011) Temporal coding in auditory cortex. In: Winer JA, Schreiner CE (eds) *The Auditory Cortex*. Springer, New York, pp 309–328
- Eilts-Grimm K, Wiese K (1984) An electrical analogue model for frequency dependent lateral inhibition referring to the omega neurons in the auditory pathway of the cricket. *Biol Cybern* 51:45–52
- Engel TA, Schimansky-Geier L, Herz AVM, Schreiber S, Erchova I (2008) Subthreshold membrane-potential resonances shape spike-train patterns in the entorhinal cortex. *J Neurophysiol* 100(3):1576–1589
- Erchova I, Kreck G, Heinemann U, Herz AVM (2004) Dynamics of rat entorhinal cortex layer II and III cells: characteristics of membrane potential resonance at rest predict oscillation properties near threshold. *J Physiol* 560(Pt 1):89–110
- Farris H, Mason A, Hoy RR (2004) Identified auditory neurons in the cricket *Gryllus rubens*: temporal processing in calling song sensitive units. *Hear Res* 193(1–2):121–133
- Faulkes Z, Pollack GS (2000) Effects of inhibitory timing on contrast enhancement in auditory circuits in crickets *Teleogryllus oceanicus*. *J Neurophysiol* 84(3):1247–1255
- Fettiplace R (1987) Electrical tuning of hair cells in the inner ear. *Trends Neurosci* 10(10):421–425
- Fullard JH, Ratcliffe JM, Guignon C (2005) Sensory ecology of predator-prey interactions: responses of the AN2 interneuron in the field cricket, *Teleogryllus oceanicus* to the echolocation calls of sympatric bats. *J Comp Physiol A* 191(7):605–618
- Gade S, Herlufsen H (1987) Use of weighting functions in DFT/FFT analysis (Part I). *Brüel Kjaer Technical Rev* 3:1–28
- Gerstein GL, Kiang NY (1960) An approach to the quantitative analysis of electrophysiological data from single neurons. *Biophys J* 1:15–28
- Gimbarzovsky B, Miura RM, Puil E (1984) Impedance profiles of peripheral and central neurons. *Can J Physiol Pharmacol* 62(4):460–462
- Goertzel G (1958) An algorithm for the evaluation of finite trigonometric series. *Am Math Mon* 65(1):34–35
- Hennig RM (1988) Ascending auditory interneurons in the cricket *Teleogryllus commodus* (Walker): comparative physiology and direct connections with afferents. *J Comp Physiol A* 163(1):135–143
- Hennig RM (2003) Acoustic feature extraction by cross-correlation in crickets? *J Comp Physiol A* 189(8):589–598
- Hennig RM (2009) Walking in Fourier's space: algorithms for the computation of periodicities in song patterns by the cricket *Gryllus bimaculatus*. *J Comp Physiol A* 195(10):971–987
- Hennig RM, Franz A, Stumpner A (2004) Processing of auditory information in insects. *Microsc Res Tech* 63(6):351–374
- Hildebrandt KJ (2014) Neural maps in insect versus vertebrate auditory systems. *Curr Opin Neurobiol* 24(1):82–87
- Horseman G, Huber F (1994) Sound localisation in crickets. I. Contralateral inhibition of an ascending auditory interneurone. *J Comp Physiol A* 175(4):389–398
- Hoy RR (1978) Acoustic communication in crickets: a model system for the study of feature detection. *Fed Proc* 37(10):2316–2323
- Hubel DH, Wiesel TN (1962) Receptive fields, binocular interaction and functional architecture in the cat's visual cortex. *J Physiol* 160:106–154
- Hutcheon B, Yarom Y (2000) Resonance, oscillation and the intrinsic frequency preferences of neurons. *Trends Neurosci* 23(5):216–222
- Hutcheon B, Miura RM, Puil E (1996) Models of subthreshold membrane resonance in neocortical neurons. *J Neurophysiol* 76(2):698–714
- Imaizumi K, Pollack GS (2001) Neural representation of sound amplitude by functionally different auditory receptors in crickets. *J Acoust Soc Am* 109(3):1247–1260
- Izhikevich EM (2001) Resonate-and-fire neurons. *Neural Netw* 14(6–7):883–894
- Jones JP, Palmer LA (1987) An evaluation of the two-dimensional gabor filter model of simple receptive fields in cat striate cortex. *J Neurophysiol* 58(6):1233–1258
- Koch C (1984) Cable theory in neurons with active, linearized membranes. *Biol Cybern* 50(1):15–33
- Kostarakos K, Hedwig B (2012) Calling song recognition in female crickets: temporal tuning of identified brain neurons matches behavior. *J Neurosci* 32(28):9601–9612
- Kostarakos K, Hedwig B (2015) Pattern recognition in field crickets: concepts and neural evidence. *J Comp Physiol A* 201(1):73–85
- Libersat F, Murray J, Hoy RR (1994) Frequency as a releaser in the courtship song of two crickets, *Gryllus bimaculatus* (de Geer) and *Teleogryllus oceanicus*: a neuroethological analysis. *J Comp Physiol A* 174:485–494
- Machens CK, Stemmler MB, Prinz P, Krahe R, Ronacher B, Herz AV (2001) Representation of acoustic communication signals by insect auditory receptor neurons. *J Neurosci* 21(9):3215–3227
- Marsat G, Pollack GS (2004) Differential temporal coding of rhythmically diverse acoustic signals by a single interneuron. *J Neurophysiol* 92(2):939–948
- Marsat G, Pollack GS (2005) Effect of the temporal pattern of contralateral inhibition on sound localization cues. *J Neurosci* 25(26):6137–6144
- Marsat G, Pollack GS (2006) A behavioral role for feature detection by sensory bursts. *J Neurosci* 26(41):10542–10547
- Nabatiyan A, Poulet JFA, de Polavieja GG, Hedwig B (2003) Temporal pattern recognition based on instantaneous spike rate coding in a simple auditory system. *J Neurophysiol* 90(4):2484–2493
- Nolen TG, Hoy RR (1984) Initiation of behavior by single neurons: the role of behavioral context. *Science* 226(4677):992–994
- Nolen TG, Hoy RR (1986) Phonotaxis in flying crickets. I. Attraction to the calling song and avoidance of bat-like ultrasound are discrete behaviors. *J Comp Physiol A* 159(4):423–439
- Pollack GS, Kim JS (2013) Selective phonotaxis to high sound-pulse rate in the cricket *Gryllus assimilis*. *J Comp Physiol A* 199(4):285–293

- Popov AV, Shuvalov VF, Markovich A (1976) The spectrum of the calling signals, phonotaxis, and the auditory system in the cricket *Gryllus bimaculatus*. *Neurosci Behav Physiol* 7:56–62
- Quiroga RQ, Nadasdy Z, Ben-Shaul Y (2004) Unsupervised spike detection and sorting with wavelets and superparamagnetic clustering. *Neural Comput* 16(8):1661–1687
- Reiss RF (1962) A theory and simulation of rhythmic behavior due to reciprocal inhibition in small nerve nets. AIEE-IRE '62 (Spring): Proceedings of the May 1–3, 1962, spring joint computer conference. ACM, New York, pp 171–194
- Rheinlaender J, Kalmring K, Popov AV, Rehbein H (1976) Brain projections and information processing of biologically significant sounds by two large ventral-cord neurons of *Gryllus bimaculatus* DeGeer (Orthoptera, Gryllidae). *J Comp Physiol A* 110(3):251–269
- Richardson MJE, Brunel N, Hakim V (2003) From subthreshold to firing-rate resonance. *J Neurophysiol* 89(5):2538–2554
- Roeder KD (1962) The behaviour of free flying moths in the presence of artificial ultrasonic pulses. *Anim Behav* 10(3–4):300–304
- Rose D, Blakemore C (1974) Effects of bicuculline on functions of inhibition in visual cortex. *Nature* 249(455):375–377
- Rössert C, Moore LE, Straka H, Glasauer S (2011) Cellular and network contributions to vestibular signal processing: impact of ion conductances, synaptic inhibition, and noise. *J Neurosci* 31(23):8359–8372
- Sabourin P, Pollack GS (2010) Temporal coding by populations of auditory receptor neurons. *J Neurophysiol* 103(3):1614–1621
- Sabourin P, Gottlieb H, Pollack GS (2008) Carrier-dependent temporal processing in an auditory interneuron. *J Acoust Soc Am* 123(5):2910–2917
- Schildberger K (1984) Temporal selectivity of identified auditory neurons in the cricket brain. *J Comp Physiol A* 155(2):171–185
- Schildberger K, Hörner M (1988) The function of auditory neurons in cricket phonotaxis: I. Influence of hyperpolarization of identified neurons on sound localization. *J Comp Physiol A* 163(5):621–631
- Schnitzler HU, Kalko EKV (2001) Echolocation by insect-eating bats. *Bioscience* 51(7):557–569
- Schreiber S, Erchova I, Heinemann U, Herz AVM (2004) Subthreshold resonance explains the frequency-dependent integration of periodic as well as random stimuli in the entorhinal cortex. *J Neurophysiol* 92(1):408–415
- Schreiber S, Samengo I, Herz AVM (2009) Two distinct mechanisms shape the reliability of neural responses. *J Neurophysiol* 101(5):2239–2251
- Schreiner CE, Langner G (1988) Coding of temporal patterns in the central auditory nervous system. In: Gerald M, Edelman WMC, Einar Gall W (eds) *Auditory function: neurobiological bases of hearing*. Wiley, New York, pp 337–361
- Schwartz O, Pillow JW, Rust NC, Simoncelli EP (2006) Spike-triggered neural characterization. *J Vis* 6(4):484–507
- Selverston AI, Kleindienst HU, Huber F (1985) Synaptic connectivity between cricket auditory interneurons as studied by selective photoinactivation. *J Neurosci* 5(5):1283–1292
- Sharafi N, Benda J, Lindner B (2013) Information filtering by synchronous spikes in a neural population. *J Comput Neurosci* 34(2):285–301
- Smith EC, Lewicki MS (2006) Efficient auditory coding. *Nature* 439(7079):978–982
- Sysel P, Rajmic P (2012) Goertzel algorithm generalized to non-integer multiples of fundamental frequency. *EURASIP J Adv Signal Process* 2012(1):1–8
- Todd BS, Andrews DC (1999) The identification of peaks in physiological signals. *Comput Biomed Res* 32(4):322–335
- Treves A (1993) Mean-field analysis of neuronal spike dynamics. *Network* 4(3):259–284
- Triblehorn JD, Ghose K, Bohn K, Moss CF, Yager DD (2008) Free-flight encounters between praying mantids (*Parasphendale agrionina*) and bats (*Eptesicus fuscus*). *J Exp Biol* 211(4):555–562
- Tunstall DN, Pollack GS (2005) Temporal and directional processing by an identified interneuron, ON1, compared in cricket species that sing with different tempos. *J Comp Physiol A* 191(4):363–372
- Urdapilleta E, Samengo I (2015) Effects of spike-triggered negative feedback on receptive-field properties. *J Comput Neurosci* 38(2):405–425
- van Hateren JH, Laughlin SB (1990) Membrane parameters, signal transmission, and the design of a graded potential neuron. *J Comp Physiol A* 166(4):437–448
- Webb B, Wessnitzer J, Bush S, Schul J, Buchli J, Ijspeert A (2007) Resonant neurons and bushcricket behaviour. *J Comp Physiol A* 193(2):285–288
- Weber T, Thorson J (1989) Phonotactic behavior of walking crickets. In: Huber F, Moore TE, Loher W (eds) *Cricket behavior and neurobiology*. Cornell UP, Ithaca, pp 310–339
- Wiese K, Eilts K (1985) Evidence for matched frequency dependence of bilateral inhibition in the auditory pathway of *Gryllus bimaculatus*. *Zool Jahrb Abt allg Zool Physiol Tiere* 89(2):181–201
- Wohlers DW, Huber F (1978) Intracellular recording and staining of cricket auditory interneurons (*Gryllus campestris* L., *Gryllus bimaculatus* DeGeer). *J Comp Physiol A* 127(1):11–28
- Wohlers DW, Huber F (1982) Processing of sound signals by six types of neurons in the prothoracic ganglion of the cricket, *Gryllus campestris* L. *J Comp Physiol A* 146(2):161–173
- Wytenbach RA, May ML, Hoy RR (1996) Categorical perception of sound frequency by crickets. *Science* 273(5281):1542–1544
- Yager DD (2012) Predator detection and evasion by flying insects. *Curr Opin Neurobiol* 22(2):201–207